Analytical Methods

ROYAL SOCIETY OF CHEMISTRY

PAPER

View Article Online
View Journal | View Issue



Cite this: *Anal. Methods*, 2021, **13**, 4105

# Electrospray deposition for single nanoparticle studies†

Gargi S. Jagdale, Myung-Hoon Choi, Natasha P. Siepser, Soojin Jeong, Yi Wang, Rebecca X. Skalla, Kaixiang Huang, Xingchen Ye and Lane A. Baker *

Single entity electrochemical (SEE) studies that can probe activities and heterogeneity in activities at nanoscale require samples that contain single and isolated particles. Single, isolated nanoparticles are achieved here with electrospray deposition of colloidal nanoparticle solutions, with simple instrumentation. Role of three electrospray (ES) parameters, *viz.* spray distance (emitter tip-to-substrate distance), ES current and emitter tip diameter, in the ES deposition of single Au nano-octahedra (Au ODs) is examined. The ES deposition of single, isolated Au ODs are analyzed in terms of percentage of single NPs and local surface density of deposition. The local surface density of ES deposition of single Au ODs was found to increase with decrease in spray distance and emitter tip diameter, and increase in ES current. While the percentage of single particle ES deposition increased with increase in spray distance and decrease in emitter tip size. No significant change in the single Au ODs ES deposition percentage was observed with change in ES current values included in this study. The most favourable conditions in the ES deposition of Au ODs in this study resulted in the local surface density of 0.26 ± 0.05 single particles per $\mu m^2$ and observation of 96.3% single Au OD deposition.

Received 30th July 2021
Accepted 17th August 2021

DOI: 10.1039/d1ay01295a

rsc.li/methods



## Introduction

Electrospray (ES) is a well-known process, in which, application of an electric potential to an electrolyte solution results in an emission of charged droplets.[1] Desolvation of the emitted droplets increases each drop's net charge and can eventually lead to Coulomb fission, which is a common approach used for ionization in mass spectrometry.[2] A significant body of work also exists on the use of electrospray as a method for deposition of molecules, polymers and nanoparticles, primarily in formats referred to independently as ultra-high vacuum (UHV) electrospray deposition[3] and soft-landing[4] (although there is significant overlap in the approaches). UHV electrospray makes use of multiple differentially pumped stages (which can span 7 orders of magnitude in pressure) to cross the electrospray to vacuum environment. For such studies, deposition onto pristine substrates has been demonstrated which provides excellent opportunities to study the structure of materials deposited, even at the atomic level.[5] Materials and molecules deposited have included large biomolecules like fibronectin,[3] large organic molecules like fullerenes[6] and porphyrins,[7] and carbon nanotubes.[8] Soft-landing techniques increase the level of control in deposition by regulating the energy of deposition with external fields and/or allowing mass selection for deposition of specific species. Deposition of large complex organic molecules,[9,10] bionanoparticles,[11] metallic clusters[12,13] have been realized by soft-landing. Studies of soft-landing at ambient pressure have been reported which further realize lower instrumental complexity and expenses.[14] Advanced applications, which include fabrication of patterned surfaces, surface modifications and reaction studies have also been carried out with ambient soft-landing methods.[15–24]

Recently, single-entity electrochemical (SEE) measurement has garnered interest for measurement of discrete entities, especially in comparison to more traditional ensemble measurements.[25–28] Perspectives and reports about SEE measurements encourage new outlooks towards preparing, handling and analysing single entities.[29–32] Electrochemical scanned probes provide an especially compelling route to SEE measurements and have shown application in assessment of biological and materials samples, including detailed studies of single electrocatalytic entities.[33–39] We have been interested in the utility of SEE approaches, including scanning electrochemical cell microscopy (SECCM),[40] to investigate the catalytic properties of metallic nanoparticles with precisely controlled surface morphologies and facets.[41] To study single-entities with sensitivity and precision, sample preparation methods that provide isolated single nanoparticles become increasingly important. Here, inspired by elegant soft-landing approaches previously described, we describe a relatively simple route to the preparation of samples suitable for SEE studies.

*Department of Chemistry, Indiana University, 800 E Kirkwood Avenue, Bloomington, IN 47408, USA. E-mail: lanbaker@indiana.edu*

† Electronic supplementary information (ESI) available. See DOI: 10.1039/d1ay01295a

In the method described, a dual barrel or a theta capillary (pipette) is used to electrospray a colloidal nanoparticle solution onto an electrode surface. No complex energetic control of deposition or mass selection is utilized, simply positional control of a pipette at an interface. We utilize a dual barrel configuration that allows use of a "good" solvent for electrospray (*e.g.* aqueous solutions of KCl and/or ethanol) and dilutions of the mother liquor used to prepare the nanoparticles without the need for additional electrolyte, which proves beneficial to surmount colligative aggregation that can be experienced in aqueous electrolytes. Additionally, dual barrel nanopipettes used here have small tip sizes (micron range), which allows electrospray driven by the applied potential without the need for backing pressure. ES flow rates in the nanolitre per minute range achieved in ES from these microscale tip sizes also result in efficient desolvation and isolation/deposition of individual nanoparticles.[42]

Coating and direct deposition methods like drop-casting, spin-coating, and electrospinning, as well as electrospray, have been explored previously for deposition of nanoparticles.[43–53] A study by Soliwoda *et al.*[48] with special relevance to the work here, described pressure-assisted electrospray for deposition of 13 nm gold nanoparticles. The study explored surface coverage obtained by increasing the duration of electrospray process. An elegant report from Ustarroz, *et al.* described deposition of mass-selected clusters synthesized in a beam source onto a carbon-coated transmission electron microscopy (TEM) grid for analysis by correlative microscopy, including SECCM.[54] In an additional recent study by Morris and co-workers,[55] a route to synthesize nanocrystals of metal–organic-framework (MOF) in aqueous environment inside the pipette tip, with controlled deposition over a TEM grid, was demonstrated. This study also established a method to estimate mass of the synthesized nanoparticles by modelling mass transport under electric field influence.

Efforts described here are specifically directed to achieving isolated single nanocrystals with electrospray deposition from colloidal NP solutions. We hypothesize that with electrospray, sub-nanoliter volume droplets containing single, isolated nanoparticles are deposited on the substrate. We demonstrate application of ES in attaining a suitable density of single, isolated nanoparticles and nanocrystals. The ES deposition method is parameterized based on three different ES parameters - spray distance, ES current and emitter size.

# Experimental

### Pipette fabrication

Borosilicate theta capillaries (Sutter Instruments, Novato, CA) with outer diameter (o. d.) 1.5 mm were pulled on a P-97 puller (Sutter Instruments) to yield pipettes with 1/1 μm, 5/5 μm and 10/10 μm tip openings. Pipettes were imaged with an FEI Quanta 600F scanning transmission electron microscope (Thermo Fisher Scientific, Hillsboro, OR). Pipette tip diameters were measured from images collected with ImageJ software (National Institutes of Health).[56]

### Chemicals and materials

Water from an ultrapure MilliQ water purification system (18.2 MΩ cm, Millipore Corp., Burlington, MA) was used for solution preparation. Potassium chloride (VWR Analytical LLC, Randor, PA) and fluorescently labelled uniform polymer microspheres (PS beads), 0.217 μm diameter (Bang Laboratories Inc., Fishers, IN) were used as received. Metallic nanocrystals, gold octahedra (Au ODs), gold truncated ditetragonal prisms (Au TDPs) and copper nanorods (Cu NRs) were synthesized, as described in the ESI (Section S1†). A platinum wire electrode (o. d. 0.127 mm, Alfa Aesar, Haverhill, MA) and glassy carbon substrate (Alfa Aesar) were used as the working and counter electrode, respectively. Glassy carbon (GC) substrates were polished and cleaned with successively finer alumina powders (1.0 micron, 0.3 micron and 0.05 micron, CH Instruments Inc., Austin, TX) following a previously described procedure.[41] PS beads were ES deposited on indium tin oxide (ITO) coated glass slides (Delta Technologies, Ltd, Loveland CO).

### Electrospray deposition setup

A schematic of the setup used is shown in Fig. 1a. A theta pipette emitter (Fig. 1b) was backfilled with solution using a microfil needle (World Precision Instruments, Sarasota, Fl). One barrel was filled with the colloidal nanoparticles solution and the second barrel was filled with an aqueous solution with 2.5 mM KCl serving as electrolyte. A platinum wire was back inserted into the nanoparticle loaded barrel for electrical connection. A high voltage power supply (Bertan, Hicksville, NY) was used to apply potential to the Pt wire. The GC substrate was placed in electrical contact with a stainless-steel plate connected to a picoammeter (414S, Keithley Instruments, Cleveland, OH) to collect current generated from electrospray. A robotic arm (DOBOT Magician, In-Position Technologies, Chandler, AZ) was employed to accurately position the pipette emitter over the GC substrate. Live video of the pipette emitter and GC substrate was monitored with a handheld wireless digital microscope (YPC-X03 Inskam, Dongguan, China) which helped to obtain accurate distance between the ES emitter tip and GC substrate (defined as the probe-to-substrate distance, $D_{ps}$) during electrospray. The GC substrate and pipette were enclosed in a humidity chamber, where the relative humidity was maintained between 11–17%.

### Sample cleaning and data analysis

An ES deposited spot at reference conditions (defined below) was rinsed with ethanol and electrochemically cleaned following the procedure detailed in an earlier study.[41] In brief, GC substrates with ES deposited nanoparticles were immersed in ethanol for 30 s and rinsed, followed by a second immersion (90 s) and rinsing step. To clean the NPs and the GC substrate further, electrochemical cycling was carried out in 100 mM $HClO_4$. With Pt mesh and Ag/AgCl (3 M KCl) electrodes serving as counter and reference electrodes, the working electrode potential was cycled twice from 0 V to −1 V *vs.* Ag/AgCl (3 M KCl) at a scan rate of 50 mV $s^{-1}$. Micrographs of cleaned samples

 

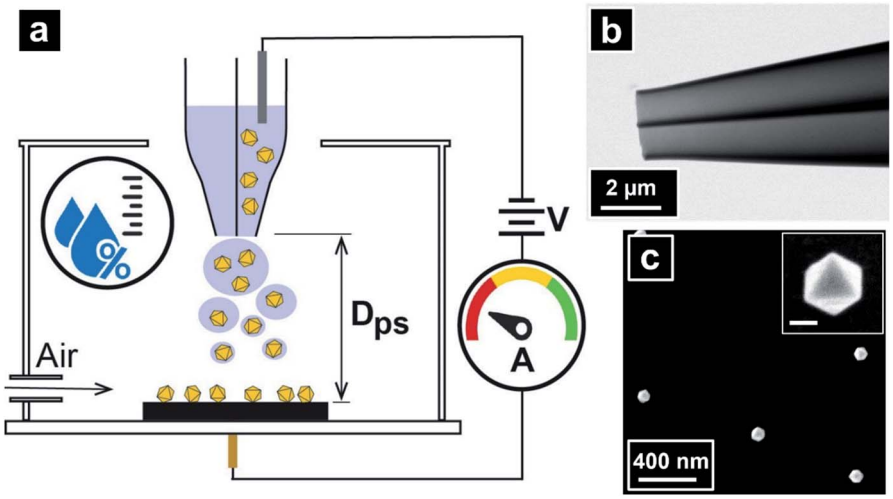


Fig. 1 (a) Schematic of the electrospray deposition setup showing a theta pipette emitter, one barrel filled with colloidal NP solution and a second barrel filled with KCl solution placed at a defined spray distance ($D_{ps}$) above the substrate on which ES deposition is carried out. Relative humidity is maintained with air flow during the experiment, while ES current generated is read on an ammeter. (b) Electron micrograph of a theta pipette emitter with tip diameter of 1 μm each barrel, and (c) electron micrograph of an electrospray deposited sample of Au ODs deposited under reference conditions and after subsequent electrochemical cleaning, with the inset showing a single OD particle (scale bar = 50 nm).

were collected with a scanning electron microscope (Zeiss Auriga 60, White Plains, NY) (other electrospray deposited samples of metallic nanoparticles were imaged with an FEI Quanta 600F). Quantification of nanoparticle deposition and additional image processing were carried out with ImageJ. The macros script in ImageJ was used to analyse the single particle distribution per unit square-micrometre (number of particles per $\mu m^2$).

ES deposited PS beads on ITO glass were covered by a cover slip and imaged by a Leica SP8 confocal microscope equipped with a 40× oil immersion objective. The wavelength of the excitation laser line was set at 490 nm and the fluorescence signal in the 500–580 nm wavelength range was collected. Brightfield and corresponding fluorescence images were captured in 4 μm × 4 μm and 20 μm × 20 μm sizes with 1024 pixels × 1024 pixels.

## Results and discussion

### Defining reference conditions for ES deposition of isolated NPs

Au nano octahedral (Au ODs) expressing predominantly {111} surface facets and an average edge length of *ca.* 99 nm were chosen as the model system to demonstrate deposition of single, isolated nanoparticles (NPs) onto a substrate *via* electrospray. Precision synthesized Au OD nanoparticles used here are nanocrystalline in nature and sample preparations that preserve the morphology are critical for subsequent electrochemical studies and catalytic measurements. As described *vide supra*, a theta pipette with two separate barrels was used as the ES emitter. A platinum wire inserted into the aqueous electrolyte barrel was used to apply a potential to generate electrospray, with electrical connection between the two barrels established in the area where the two barrels come in contact at the pipette tip. This approach allows use of both a solution favourable for electrospray and a suitable solvent system favourable for reducing nanoparticle aggregation (in the colloidal NP solution).

ES operational parameters including NP concentration, electrolyte concentration, relative humidity (RH), ES emitter tip size, spray distance ($D_{ps}$) and ES current were examined and optimized to define one reference condition for electrospray deposition which achieved reasonable surface density of single NPs on the glassy carbon substrate. The reference condition defined here, under which deposition of single Au ODs was routinely achieved is as follows: theta pipette emitter where the tip diameter of each barrel is 1 μm, one barrel of the pipette filled with a freshly prepared solution of Au ODs (diluted in water to an optical density (O. D.) of 0.33 from stock solution (O. D. = 75)) without any added electrolyte, second barrel of the pipette filled with aqueous 2.5 mM KCl solution, 11–17% RH, 2 mm spray distance ($D_{ps}$) and 8 nA of ES current. Relative humidity between 11–17% was maintained to secure repeatable electrospray operation. In the absence of humidity control, reproducible conditions were difficult or impossible to obtain. The lower RH inside the chamber (relative to ambient conditions) also helped to enhance the desolvation process in droplets produced during electrospray. In each trial, electrospray deposition was performed for a fixed time interval of 15 min. An electron micrograph of the spot from electrospray deposition on the GC substrate is shown in Fig. 2a. GC was chosen as a substrate due to the inherent low surface roughness, good electrical conductivity, and low activity for catalytic reactions that are of future interest for single NP studies.

For the reference condition, the deposited spot area obtained was observed as *ca.* 7.94 $mm^2$, and the overall circular contrast observed arises from salt that is co-deposited with Au ODs. Generally, when compared to drop-cast samples, shown in

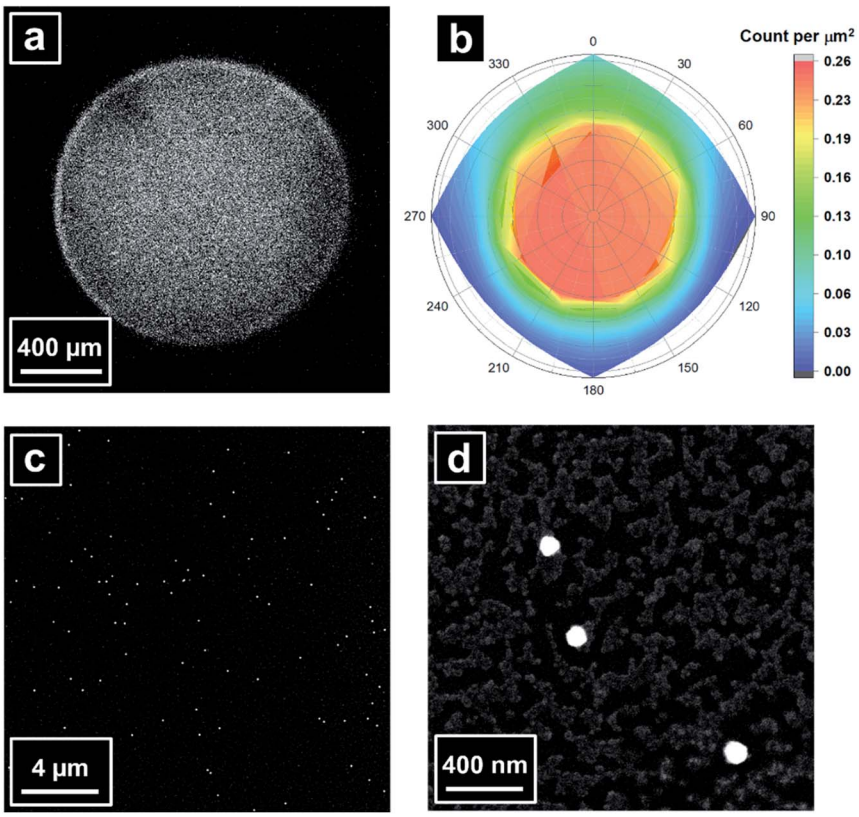


Fig. 2 (a) Electron micrograph of an ES deposition spot (diameter = 1.3 mm) at reference condition (described in text). (b) Map representing the distribution of single Au ODs per $\mu m^2$ within the ES deposition spot. Electron micrographs of (c) a 20 μm × 20 μm area from the centre of the spot were dispersed Au ODs can be seen and (d) a 2 μm × 2 μm region that show single Au ODs deposited with salt residues (grey contrast).

Fig. S2,† the ES deposition procedure was found to provide a more reproducible and controlled route to obtain uniform, single and isolated NPs onto a substrate, and further to direct the location of deposition to specific regions of the substrate. With conventional methods like drop-cast, drying solvent from the deposited drop can be difficult to control, and therefore the deposition results are hard to reproduce, and aggregation of the deposited nanoparticles is inevitable. Moreover, achieving a high percentage of single, isolated particles is difficult with drop-casting. ES deposition allows selection of solvent composition, extent of desolvation and density of nanoparticle deposition.

Distribution of single NPs inside the deposited spot was determined by analysis of four replicate electrospray deposited spots ($n = 4$). As demonstrated from Fig. S3,† 13 electron micrographs were taken from each of the four ES deposited spots (one micrograph at the centre, three more taken moving outward in each of the four directions from centre, top (T), bottom (B), left (L) and right (R)), with each micrograph separated by *ca.* 200 μm. The area of each micrograph was 480 $\mu m^2$. As the goal of this method is to prepare single and isolated NPs, the number of single NPs, aggregates of 2 NP and aggregates with >2 NPs in each SEM image were counted with ImageJ. The distribution of single NPs in the ES deposited spots was characterized as number of single particles per square-micrometre (number of particles per $\mu m^2$) (Fig. 2b). Details of the analysis are included in ESI.† The number of single ODs deposited was highest at the centre of the ES deposited area (*ca.* 0.26 ± 0.05 NPs per $\mu m^2$) and decreased radially from the centre of the spot. Close to zero NPs were observed at edges in three directions (bottom (B), left (L) and right (R)), with only salt deposits observed. The L to R direction (see ESI for description†) in Fig. 2b corresponds to the direction parallel to the septum of the pipette dividing the two barrels of the theta emitter. The asymmetry of the emitter tip is reflected in the distribution of deposited particles. The surface density distribution of deposited single Au ODs is a skewed Gaussian curve, with a shift in more dense OD deposition in area the emitter barrel (defined as top (T) here) containing the colloidal NP solution was over.

A representative SEM image, taken from the centre region of an ES deposition spot for the reference condition is shown in Fig. 2c. Center regions from four replicate deposition spots were analysed to understand the nanoparticle deposition characteristics, *viz.* single particle percentage and uniformity in the surface density of deposited NPs. At reference conditions, salt from electrolyte was observed to be deposited with a thin uniform layer over the GC substrate, and can be seen as grey contrast in Fig. 2d. Note, the Au ODs deposited have a covering of residual salt. However, thorough cleaning of the sample, as described previously, results in reduction/removal of both salt and ligand residues from the deposited Au ODs (Fig. 1c shows an electron micrograph of electrospray deposited Au ODs

 

sample after ethanol and electrochemical cleaning treatments). Salt and ligand residues appear to be removed, with Au OD nanocrystal morphology unaltered. A recent study that includes detailed analysis on removal of ligands from deposited nanoparticle surfaces on a GC substrate with electrochemical cleaning can be referred.[57]

### Characterization of operational parameters dependent electrospray deposition of Au OD nanocrystals

After establishing the reference condition for electrospray deposition with the Au OD system, a systematic study of the electrospray deposition of single Au ODs was carried out by changing electrospray operational parameters. For all conditions, single particle surface density, uniformity in the local surface density, aggregation percentage and presence of residual salts were analysed. Single particle surface density of the sample was visualized by counting the number of single particles per $\mu m^2$ at the centre region of the ES deposited spot following the protocol described above. To quantify the uniformity in the local surface density of deposited single Au ODs, a 480 $\mu m^2$ electron micrograph was divided into 4 $\mu m \times 4$ $\mu m$ areas, and the nature of particle distribution was counted with values binned as single (an isolated NP), two (two NPs touching), and >two (any other distribution of NPs). The average and standard deviation values were then converted to obtain values representing the number of NPs per square micrometre. The average value is reported as the particle count per $\mu m^2$ and the average of standard deviation, from each of the four trials, represents uniformity in the local surface density of deposited particles. In all the following figures, red error bars are the standard deviation from four replicate ES deposited spots ($n = 4$) and black error bars represent the uniformity in the number of particles deposited per square micrometres (total 4 $\mu m \times 4$ $\mu m$ areas, $n = 120$). The percentage of single Au ODs deposited in the centre areas is calculated using the following equation:

$$\text{Single particle\%} = \frac{\text{Single particle} \times 100}{\text{Single particles} + \text{aggregated particles}} \quad (1)$$

Uniformity in the local surface density (LSD) of deposited single particles can be better visualized by variation in the average surface density of single particles deposited and was calculated with the equation:

$$\text{Variation in LSD\%} = \frac{\text{Range of single NP surface density}}{\text{Average single NP surface density}} \times 100 \quad (2)$$

First, Au OD deposition at different spray distances ($D_{ps}$), *i.e.*, the distance between the ES emitter tip and the substrate, was studied. Electron micrographs were taken at the centre regions of the ES deposited spots at spray distances 0.5, 2.0 and 3.5 mm (Fig. 3a–c). Four replicates were performed for each $D_{ps}$. As the $D_{ps}$ increased the overall surface density of Au ODs deposited decreased, and the size of deposited salt residues was observed. Reduction in the size of salt residue droplets is attributed to the increased flight-time experienced by the droplets produced in electrospray generated at the emitter tip. The longer flight-time helps aid solvent evaporation, resulting in higher droplet fission events, which forms smaller droplets. Further the spray cone is extended, which results in a larger spread of the ES deposited spot area. A similar trend was observed in a recent study by Marsh *et al.*[58] where the reaction extent to form phenylhydrazone from isatin was studied by examining the ES droplets deposited onto a substrate. For NPs studied here, the highest

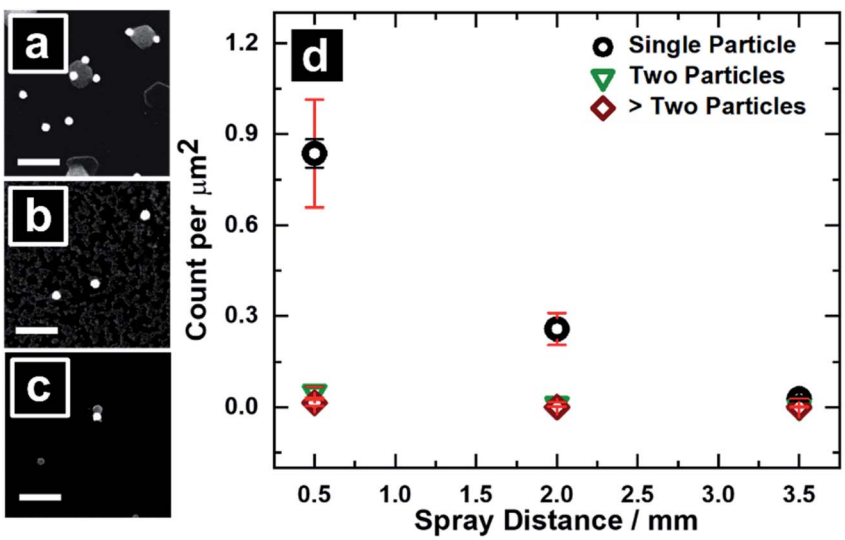


Fig. 3 Electron micrographs of ES deposition of Au ODs with spray distances of (a) 0.5 mm, (b) 2 mm and (c) 3.5 mm (scale bar on all three micrographs = 500 nm); (d) quantitative representation of number of NPs per $\mu m^2$ at different spray distances, red error bars represent variation between replicate trials, black error bars represent variation in local surface density of NPs ES deposited.

surface density in ES deposition of single Au ODs was obtained at the closest spray distance ($D_{ps}$ = 0.5 mm), with a coverage of 0.84 ± 0.18 single ODs per μm$^2$, compared to 0.26 ± 0.05 and 0.03 ± 0.003 single ODs per μm$^2$ at 2 and 3.5 mm spray distances, respectively (Fig. 3d). Aggregates containing two (green triangle) or more (red diamond) particles for all three spray distances were negligible, with the highest aggregate count observed for the closest spray distance (*ca.* 0.06 ± 0.02 aggregated ODs per μm$^2$ for 0.5 mm $D_{ps}$). The local surface density uniformity and aggregation extent are expressed in percentages in Table S1.† Under these conditions, a favourable deposition of single Au ODs was obtained for the reference conditions with 96.3% single Au ODs of the deposited NPs and a variation of 8.8% in the local surface density at the centre of the ES deposited spot.

Next, ES current at which Au ODs were deposited was examined. To determine the range of stable ES current values for the Au OD ES deposition, current–potential (*I–V*) curves were recorded to determine the onset of electrospray and general trends in current relative to applied potential. An averaged *I–V* response ($n$ = 3) for typical 1/1 μm theta pipettes is shown in Fig. 4a. Current–voltage responses from the three individual pipettes are shown in Fig. S5a† (also inset in Fig. 4a). Three current values, 2 nA (black line), 4 nA (blue line) and 8 nA (green line) close to the ES onset were chosen for this study. We observed that reproducibility of ES deposition of single NPs is lost at higher currents further away from the onset potential for ES. Furthermore, note from the inset in Fig. 4a, the standard deviation in the measured current for individual pipettes increase above ~10 nA, *i.e.* ES current is observed to be less stable. Fig. S5(b–d)† shows electron micrographs corresponding to the three ES current values used for deposition. As the ES current increases, the size of salt residues observed decreases. Fig. 4b quantitatively demonstrates the deposition of Au ODs at the three different ES currents. The highest surface density of single Au ODs deposition was obtained at 8 nA (0.26 ± 0.05 single ODs per μm$^2$, this is also the reference condition described previously), while the lowest surface density of 0.10 ± 0.03 single Au ODs per μm$^2$ was observed at 2 nA ES current. Additionally, uniformity in the local surface density of ES deposited single Au ODs was the highest for 8 nA. Generally, both a favourable surface density and better uniformity in the local density of deposited single Au ODs was obtained at higher ES currents. Higher potentials are applied to achieve higher ES currents and thus, the initial droplets formed in electrospray process would carry higher charge and undergo more fission events, with all other parameters held constant. The flow rate would also be higher for higher current. Taken together, these effects result in smaller sizes for salt residue deposits and larger number of single Au ODs deposited at higher currents. However, as mentioned earlier, there is a limit to the ES current at which stable deposition is obtained, without reducing the

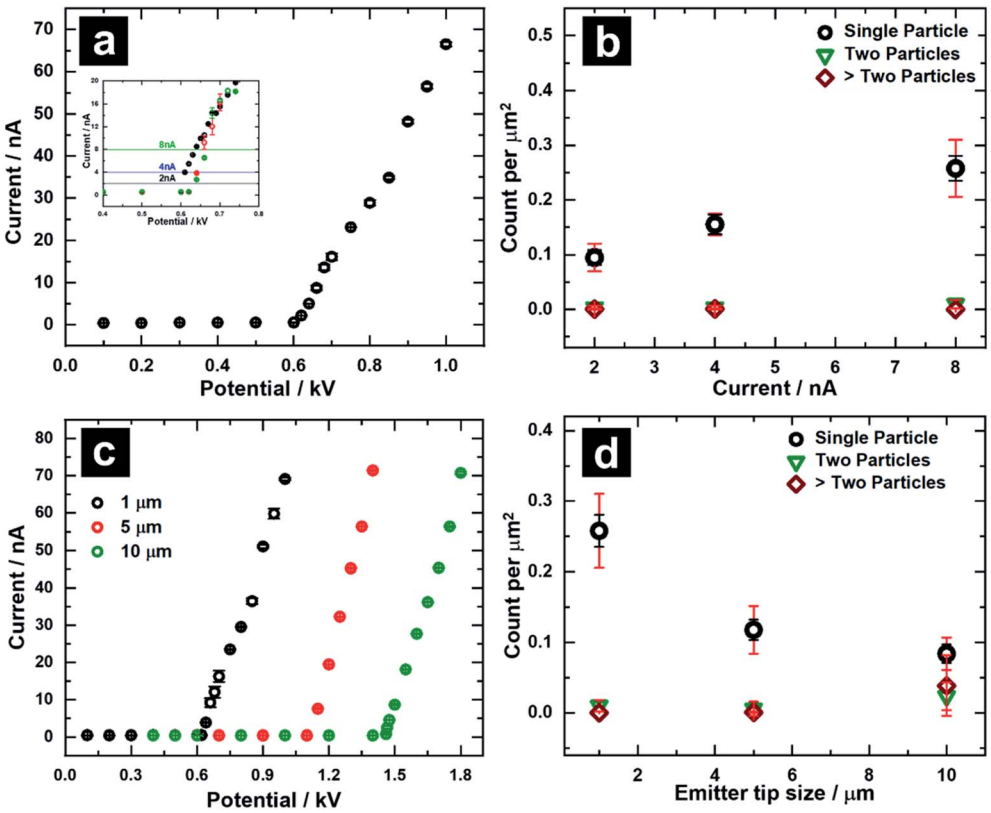


Fig. 4 (a) Average *I–V* response from 1/1 μm electrospray emitter ($n$ = 3). Inset shows zoomed part of *I–V* responses from three individual pipettes around the ES current values used in the study (horizontal lines black – 2 nA, blue – 4 nA, green – 8 nA). (b) Particles per μm$^2$ at different ES currents. (c) *I–V* response for different sized ES emitters, and (d) plot of particles per μm$^2$ for different sizes of ES emitter.

 

quality of single NP deposition and tip clogging due to NP aggregation inside the pipette. Single Au OD deposition% at all three current values were found to be similar and ranged between 95.8% and 97.1% (Table S1†). However, the uniformity in local surface density of deposited particles increased at higher currents, with the lowest variation of 8.8% at 8 nA.

The role of theta pipette emitter size in the deposition nature of NPs was examined. Diameters of theta pipettes used were 1/1 μm, 5/5 μm and 10/10 μm (Fig. S6a–c†). A comparison of corresponding *I–V* responses from the three different tip sizes is shown in Fig. 4c. As observed in the *I–V* response, the potential required to induce an electrospray increased with increasing emitter size. The potential required to maintain a stable ES current of 8 nA was applied for all the three sizes. As expected, salt residues increased in size with larger emitter pipette diameters. The highest surface density of single Au ODs deposited was achieved with the 1/1 μm emitter. The % single particle deposition obtained with 5/5 μm tip emitter (94.9%) was comparable with the 1/1 μm tip emitter (96.3%), however, the surface density of deposited NPs was lower. For the 10/10 μm tip emitter, both surface density and % single particles observed (57.5%) were lower than for emitters with smaller tip sizes. Larger aggregates with more than 3 particles, not observed in other conditions of ES depositions examined here, were observed for 10/10 μm emitters. Deposited salt residues were larger in size and distributed more sparsely as the emitter size increased, in agreement with the presumed increase in droplet size, leading to less efficient desolvation for larger diameter emitters. The Coulomb fission that occurs in a parent droplet to produce progeny droplets can be represented with the equation by Rayleigh (eqn (3)),[59] that related the charge to emitter radius.

$$Q_{\mathrm{Ry}} = 8\pi(\varepsilon_0 \gamma r^3)^{1/2} \quad (3)$$

In the equation, $Q_{\mathrm{Ry}}$ is the charge on the droplet, $\varepsilon_0$ is electrical permittivity, $\gamma$ is surface tension of the solvent and $r$ is radius of the droplet. A recent report has described fluorescence measurements of the electrospray desolvation process for emitters with diameters of nominally 5 and <1 μm.[60] In this study, the emitter diameter was found to have a strong influence on the ability – notably of aqueous solutions – to produce desolvated proteins. ES deposition of NPs presents a challenge relative to protein deposition, as emitters with tip dimensions of the tip can approach or even be smaller than the NPs being deposited,[61] which is obvious deleterious to deposition. The use of smaller tip electrospray emitters was found to generate smaller charged droplets that needed to undergo fewer Coulomb fission events to result in desolvated ions. Based on results here, we hypothesize that for the case of the smallest diameter tips (1 μm/1 μm) used, either from initial droplet formation or through droplet fission events, desolvation is favourable for individual NPs per droplet, which results in deposition of single, isolated NPs. For larger diameter emitters, multiple NPs are likely present in each droplet, which is also not completely desolvated under short travel times used here, to result in multiple NPs per droplet, often observed encased together with residual salt (see Fig. S6i†).

### Generality of the process for single nanocrystal/nanoparticle deposition

To examine the general utility of the approach described here, different types of nanoparticles were deposited with ES. The first example is of gold nanocrystals with the shape of truncated ditetragonal prisms (Au TDPs, primary axis length *ca.* 83 nm). Fig. 5a shows the general density of Au TDPs obtained with ES deposition at conditions similar to the reference conditions used for Au ODs. In Fig. 5b, a region of 2 μm × 2 μm of ES deposition with an inset of the Au TDP nanoparticle after ES deposition is shown. A good deposition of complex shaped NPs was demonstrated with Au TDPs while retaining the original morphology after electrospray.

A second example of nanoparticles chosen were copper nanorods (Cu NRs) with axis lengths ranging from 200 to 400 nm.[62] This sample proves more challenging due to several aspects: (1) preserving the hight aspect ratio of NRs, and (2) Cu NRs are dispersed in toluene, a solvent which proves difficult for generating an electrospray. Large emitter tips with size 5/5 μm were used to mitigate NR aggregation at the emitter tip. Cu NRs in toluene were back-filled inside one barrel of the theta pipette emitter, and a mixture solvent of 20 : 80 v/v% ethanol : toluene (without added electrolyte) was back-filled in the second barrel. ES deposition was carried out by application of 3 kV potential for 40 s. The resultant ES deposited Cu NRs are shown in Fig. 5c and d. Note that the centre of the deposited spots for Cu NRs showed significant residual material from the mother liquor, however, isolated single Cu NRs with reasonably low residual material can be observed in the ring area around the edges of the deposited spots.

A third nanoparticle type demonstrated here is polystyrene (PS) beads with attached fluorophores. PS beads (220 nm

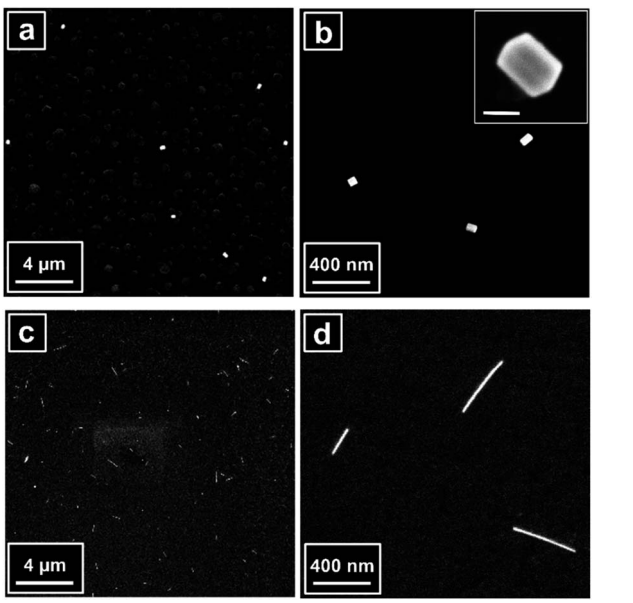


Fig. 5 Electron micrographs of electrospray deposited single nanocrystals; (a and b) Au TDPs (scale bar on inset in (b) is 50 nm) and (c and d) Cu NRs.

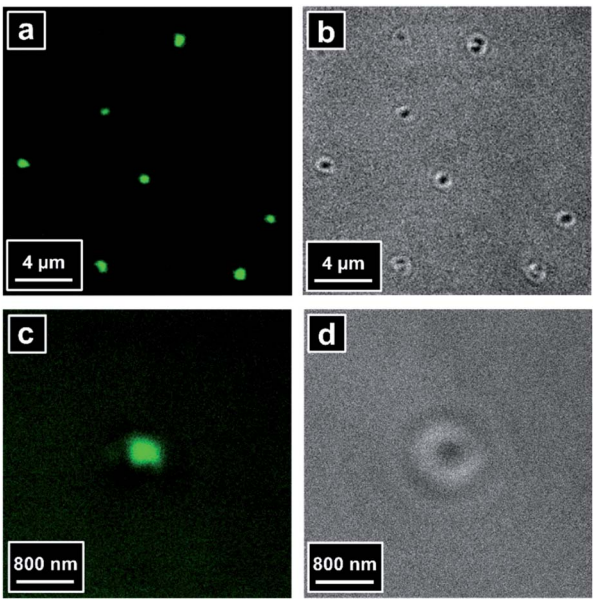


Fig. 6 Confocal fluorescence micrographs (a and c) and corresponding bright field micrographs (b and d) of electrospray deposited 220 nm diameter polystyrene beads.

diameter) were prepared in pure $H_2O$ at a similar concentration to the Au ODs concentration (0.96 particles per pL) and were ES deposited onto an ITO-coated slide (for optical transparency) and imaged with confocal microscopy. No added electrolyte was used in the second barrel for the ES of PS beads since aggregation of the beads was observed when KCl electrolyte solution was introduced from the second barrel. The resultant fluorescence and brightfield images, Fig. 6, show predominantly single PS beads depositions with some dimers deposited under the reference conditions of ES operation used in the deposition of single Au ODs. Results on ITO also show the general applicability of the approach described here to substrates beyond GC, although fine tuning dependent on substrate properties.

## Conclusions

Inspired from ambient soft-landing method, we have demonstrated a simple, efficient method to obtain deposition of single, isolated nanoparticles with electrospray at ambient conditions. Employing Au ODs as our model nanoparticle system, the nature of deposition at different electrospray conditions, namely spray distance, ES current and ES emitter size was studied. The systematic study shows that the experimental parameters can be tuned to achieve the desired deposition result. Furthermore, we demonstrate this method to obtain monodispersed deposition of three different types of nanoparticles – Au TDPs, Cu NRs, and PS beads. With control over the ES deposition operational parameters, a thin film of nanoparticles can also be achieved in applications where required. We believe that this simple method to prepare samples with single nanoparticles will have wide applications in SEE measurements, surface modification experiments, and much more.

## Author contributions

Conceptualization, G. S. J., M. C., N. P. S., and L. A. B; methodology, G. S. J., M. C., N. P. S., S. J., Y. W. and R. X. S; validation, G. S. J., M. C., N. P. S., S. J., K. H., X. Y, and L. A. B.; formal analysis, G. S. J. and L. A. B; investigation, G. S. J., M. C., S. J. and K. H.; writing – original draft, G. S. J. and L. A. B., writing – review and editing, G. S. J., M. C., N. P. S., S. J., K. H., X. Y. and L. A. B.; supervision, X. Y. and L. A. B.; funding acquisition, X. Y. and L. A. B.

## Conflicts of interest

There are no conflicts to declare.

## Acknowledgements

Support from National Science Foundation (CHE-1808133, L. A. B and DMR-2102526, X. Y.) are acknowledged. Additional support to L. A. B. from the Johnson Center for Innovation and Translational Research, which is part of the Indiana University Innovation and Commercialization Office is acknowledged. The Nanoscale Characterization Facility (NCF) and Light Microscopy Imaging Center (LMIC) of Indiana University, Bloomington, are acknowledged for access to instrumentation, including electron microscopy supported by the National Science Foundation MRI program (CHE-0923064).

## References

1 J. Rosell-Llompart, J. Grifoll and I. G. Loscertales, *J. Aerosol Sci.*, 2018, **125**, 2–31.
2 J. B. Fenn, M. Mann, C. K. Meng, S. F. Wong and C. M. Whitehouse, *Science*, 1989, **246**, 64–71.
3 E. Fornari, C. J. Roberts, R. H. Temperton and J. N. O'Shea, *J. Colloid Interface Sci.*, 2015, **453**, 252–259.
4 V. Franchetti, B. H. Solka, W. E. Baitinger, J. W. Amy and R. G. Cooks, *Int. J. Mass Spectrom. Ion Phys.*, 1977, **23**, 29–35.
5 A. Hinaut, T. Meier, R. Pawlak, S. Feund, R. Johr, S. Kawai, T. Glatzel, S. Decurtins, K. Mullen, A. Narita, S. X. Liu and E. Meyer, *Nanoscale*, 2018, **10**, 1337–1344.
6 C. J. Satterley, L. M. A. Perdigão, A. Saywell, G. Magnano, A. Rienzo, L. C. Mayor, V. R. Dhanak, P. H. Beton and J. N. O'Shea, *Nanotechnology*, 2007, **18**, 455304.
7 A. Hinaut, R. Pawlak, E. Meyer and T. Glatzel, *Beilstein J. Nanotechnol.*, 2015, **6**, 1927–1934.
8 J. N. O'Shea, J. B. Taylor, J. C. Swarbrick, G. Magnano, L. C. Mayor and K. Schulte, *Nanotechnology*, 2007, **18**, 035707.
9 S. Rauschenbach, R. Vogelgesang, N. Malinowski, J. W. Gerlach, M. Benyoucef, G. Costantini, Z. Deng, N. Thontasen and K. Kern, *ACS Nano*, 2009, **3**, 2901–2910.
10 G. Rinke, S. Rauschenbach, S. Schrettl, T. N. Hoheisel, J. Blohm, R. Gutzler, F. Rosei, H. Frauenrath and K. Kern, *Int. J. Mass Spectrom.*, 2015, **377**, 228–234.
11 V. A. Mikhailov, T. H. Mize, J. L. Benesch and C. V. Robinson, *Anal. Chem.*, 2014, **86**, 8321–8328.
12 G. E. Johnson, C. Wang, T. Priest and J. Laskin, *Anal. Chem.*, 2011, **83**, 8069–8072.

 

13 G. E. Johnson, R. Colby, M. Engelhard, D. Moon and J. Laskin, *Nanoscale*, 2015, **7**, 12379–12391.
14 A. K. Badu-Tawiah, C. Wu and R. G. Cooks, *Anal. Chem.*, 2011, **83**, 2648–2654.
15 M. Wleklinski, D. Sarkar, A. Hollerbach, T. Pradeep and R. G. Cooks, *Phys. Chem. Chem. Phys.*, 2015, **17**, 18364–18373.
16 P. A. Kottke, J. Y. Lee, A. P. Jonke, C. A. Seneviratne, E. S. Hecht, D. C. Muddiman, M. P. Torres and A. G. Fedorov, *Anal. Chem.*, 2017, **89**, 8981–8987.
17 H. Fang, D. Wang, L. Yuan, X. Wu, H. Guo, H. Chen, K. Huang and S. Feng, *New J. Chem.*, 2017, **41**, 2878–2882.
18 J. Hou, Q. Zheng, A. K. Badu-Tawiah, C. Xiong, C. Guan, S. Chen, Z. Nie, D. Wang and L. Wan, *Chem. Commun.*, 2016, **52**, 13660–13663.
19 Q. He, A. K. Badu-Tawiah, S. Chen, C. Xiong, H. Liu, Y. Zhou, J. Hou, N. Zhang, Y. Li, X. Xie, J. Wang, L. Mao and Z. Nie, *Anal. Chem.*, 2015, **87**, 3144–3148.
20 Z. Baird, P. Wei and R. G. Cooks, *Analyst*, 2015, **140**, 696–700.
21 P. Pompach, O. Benada, M. Rosulek, P. Darebna, J. Hausner, V. Ruzicka, M. Volny and P. Novak, *Anal. Chem.*, 2016, **88**, 8526–8534.
22 A. K. Badu-Tawiah, D. I. Campbell and R. G. Cooks, *J. Am. Soc. Mass Spectrom.*, 2012, **23**, 1077–1084.
23 A. K. Badu-Tawiah, J. Cyriac and R. G. Cooks, *J. Am. Soc. Mass Spectrom.*, 2012, **23**, 842–849.
24 A. Li, Z. Baird, S. Bag, D. Sarkar, A. Prabhath, T. Pradeep and R. G. Cooks, *Angew Chem. Int. Ed. Engl.*, 2014, **53**, 12528–12531.
25 F. Li, X. V. Medvedeva, J. J. Medvedev, E. Khairullina, H. Engelhardt, S. Chandrasekar, Y. Guo, J. Jin, A. Lee, H. Thérien-Aubin, A. Ahmed, Y. Pang and A. Klinkova, *Nat. Catal.*, 2021, **4**, 479–487.
26 R. J. Yu, S. W. Xu, S. Paul, Y. L. Ying, L. F. Cui, H. Daiguji, W. L. Hsu and Y. T. Long, *ACS Sens.*, 2021, **6**, 335–339.
27 R. Miao, L. Shao and R. G. Compton, *Nano Res.*, 2021, DOI: 10.1007/s12274-021-3353-8.
28 P. Pandey, G. Ghimire, J. Garcia, A. Rubfiaro, X. Wang, A. Tomitaka, M. Nair, A. Kaushik and J. He, *ACS Sens.*, 2021, **6**, 340–347.
29 Y. Wang, X. Shan and N. Tao, *Faraday Discuss.*, 2016, **193**, 9–39.
30 L. A. Baker, *J. Am. Chem. Soc.*, 2018, **140**, 15549–15559.
31 Y.-L. Ying, J. Wang, A. R. Leach, Y. Jiang, R. Gao, C. Xu, M. A. Edwards, A. D. Pendergast, H. Ren, C. K. T. Weatherly, W. Wang, P. Actis, L. Mao, H. S. White and Y.-T. Long, *Sci. China: Chem.*, 2020, **63**, 589–618.
32 A. Sekretareva, *Sensors and Actuators Reports*, 2021, **3**, DOI: 10.1016/j.snr.2021.100037.
33 F. M. Boldt, J. Heinze, M. Diez, J. Petersen and M. Borsch, *Anal. Chem.*, 2004, **76**, 3473–3481.
34 X. Shan, I. Diez-Perez, L. Wang, P. Wiktor, Y. Gu, L. Zhang, W. Wang, J. Lu, S. Wang, Q. Gong, J. Li and N. Tao, *Nat. Nanotechnol.*, 2012, **7**, 668–672.
35 C. L. Bentley, M. Kang and P. R. Unwin, *J. Am. Chem. Soc.*, 2017, **139**, 16813–16821.
36 T. Tarnev, H. B. Aiyappa, A. Botz, T. Erichsen, A. Ernst, C. Andronescu and W. Schuhmann, *Angew Chem. Int. Ed. Engl.*, 2019, **58**, 14265–14269.
37 O. J. Wahab, M. Kang and P. R. Unwin, *Curr. Opin. Electrochem.*, 2020, **22**, 120–128.
38 T. Quast, H. B. Aiyappa, S. Saddeler, P. Wilde, Y. T. Chen, S. Schulz and W. Schuhmann, *Angew Chem. Int. Ed. Engl.*, 2021, **60**, 3576–3580.
39 H. Shen, W. Xu and P. Chen, *Phys. Chem. Chem. Phys.*, 2010, **12**, 6555–6563.
40 M. E. Snowden, A. G. Guell, S. C. Lai, K. McKelvey, N. Ebejer, M. A. O'Connell, A. W. Colburn and P. R. Unwin, *Anal. Chem.*, 2012, **84**, 2483–2491.
41 M. Choi, N. P. Siepser, S. Jeong, Y. Wang, G. Jagdale, X. Ye and L. A. Baker, *Nano Lett.*, 2020, **20**, 1233–1239.
42 M. M. Mattias Wilm, *Anal. Chem.*, 1996, **68**, 1–8.
43 Z. Y. Brown N, G. K. German, X. Yong and P. R. Chiarot, *J. Electrost.*, 2017, **90**, 67–73.
44 Y. T. Guntern, V. Okatenko, J. Pankhurst, S. B. Varandili, P. Iyengar, C. Koolen, D. Stoian, J. Vavra and R. Buonsanti, *ACS Catal.*, 2021, **11**, 1248–1295.
45 E. Czechowska, K. Ranoszek-Soliwoda, E. Tomaszewska, A. Pudlarz, G. Celichowski, D. Gralak-Zwolenik, J. Szemraj and J. Grobelny, *Colloids Surf., B*, 2018, **171**, 707–714.
46 J. Eklof, T. Gschneidtner, S. Lara-Avila, K. Nygard and K. Moth-Poulsen, *RSC Adv.*, 2016, **6**, 104246–104253.
47 R. Ahmad, O. S. Wolfbeis, Y.-B. Hahn, H. N. Alshareef, L. Torsi and K. N. Salama, *Mater. Today Commun.*, 2018, **17**, 289–321.
48 K. Soliwoda, M. Rosowski, E. Tomaszewska, B. Tkacz-Szczesna, G. Celichowski and J. Grobelny, *Colloids Surf., A*, 2015, **486**, 211–217.
49 A. Tycova, J. Prikryl, A. Kotzianova, V. Datinska, V. Velebny and F. Foret, *Electrophoresis*, 2021, **42**, 103–121.
50 M. Morga, M. Nattich-Rak, M. Ocwieja and Z. Adamczyk, *Phys. Chem. Chem. Phys.*, 2019, **21**, 6535–6543.
51 L. M. Rossi, J. L. Fiorio, M. A. S. Garcia and C. P. Ferraz, *Dalton Trans.*, 2018, **47**, 5889–5915.
52 L. Lei, A. R. Gamboa, C. Kuznetsova, S. Littlecreek, J. Wang, Q. Zou, J. D. Zahn and J. P. Singer, *Sci. Rep.*, 2020, **10**, 17290.
53 Y. Zhu and P. R. Chiarot, *J. Mater. Sci.*, 2019, **54**, 6122–6139.
54 J. Ustarroz, I. M. Ornelas, G. Zhang, D. Perry, M. Kang, C. L. Bentley, M. Walker and P. R. Unwin, *ACS Catal.*, 2018, **8**, 6775–6790.
55 P. D. Morris, I. J. McPherson, M. A. Edwards, R. J. Kashtiban, R. I. Walton and P. R. Unwin, *Angew Chem. Int. Ed. Engl.*, 2020, **59**, 19696–19701.
56 W. S. Rasband, *Image Processing with ImageJ*, U.S. National Institute of Health, Bethesda, Maryland, USA.
57 M. H. Choi, S. Jeong, Y. Wang, S. J. Cho, S. I. Park, X. Ye and L. A. Baker, *Langmuir*, 2021, **37**, 7701–7711.
58 B. M. Marsh, K. Iyer and R. G. Cooks, *J. Am. Soc. Mass Spectrom.*, 2019, **30**, 2022–2030.
59 L. Rayleigh, *Philos. Mag.*, 1882, **14**, 184–186.
60 P. Tiwari, M. F. Czar and R. Zenobi, *Anal. Chem.*, 2021, **93**, 3635–3642.
61 E. M. Yuill, N. Sa, S. J. Ray, G. M. Hieftje and L. A. Baker, *Anal. Chem.*, 2013, **85**, 8498–8502.
62 S. Jeong, Y. Liu, Y. Zhong, X. Zhan, Y. Li, Y. Wang, P. M. Cha, J. Chen and X. Ye, *Nano Lett.*, 2020, **20**, 7263–7271.